PHILOSOPHICAL TRANSACTIONS OF THE ROYAL SOCIETY A MATHEMATICAL, PHYSICAL & ENGINEERING SCIENCES

Characteristics of the Defocused Spherical Fabry-Perot Interferometer as a Quasi-Linear Dispersion Instrument for High Resolution Spectroscopy of Pulsed Laser Sources

D. J. Bradley and C. J. Mitchell

Phil. Trans. R. Soc. Lond. A 1968 **263**, 209-223
doi: 10.1098/rsta.1968.0012

CHARACTERISTICS OF THE DEFOCUSED SPHERICAL FABRY–PÉROT INTERFEROMETER AS A QUASI-LINEAR DISPERSION INSTRUMENT FOR HIGH RESOLUTION SPECTROSCOPY OF PULSED LASER SOURCES

By D. J. Bradley and C. J. Mitchell

Department of Pure and Applied Physics, School of Physics and Applied Mathematics, The Queen's University of Belfast

(*Communicated by S. Tolansky, F.R.S.—Received* 4 *December* 1967—*Read* 23 *May* 1968)

[Plates 1 and 2]

CONTENTS

Defocused spherical mirror Fabry–Pérot etalons, in which the mirror separation is slightly less than the common radius of curvature, produce a multiple-beam fringe pattern of concentric rings, with quasi-linear spectral dispersion over an appreciable annular region corresponding to two free spectral ranges. The characteristics of these interferograms are discussed in relation to their many advantages for pulsed laser spectroscopy.

These advantages include: (i) accuracy of frequency difference measurement; (ii) high illumination of the detector with moderate energy density in the laser beam; (iii) ease of alinement and permanent adjustment of the mirrors leading to the attainment in practice of a very high instrumental finesse (N_R values of up to 90 have been achieved); (iv) measurement of degree of spatial coherence of laser beam; (v) ease of matching the interferogram to the spatial resolution of the detector.

A simple optical path relation determines the positions of the fringes and the location of the quasi-linear dispersion region. The interfering wavefronts, formed by multiple reflexion, have been numerically computed and summed to provide information on the finesse, fringe profiles, contrast and optimum conditions of use of this new, very high resolving power (10^7 to 10^8) quasi-linear spectrographic disperser. Constructional details are described and optical design criteria are discussed, together with the various experimental arrangements for employing the instrument. Comparison is made with the equivalent confocal and plane Fabry–Pérot etalons and methods of simultaneously measuring the temporal and spatial coherence properties of laser beams are discussed and illustrated.

Vol. 263. A. 1140. (Price £1. 5s.; U.S. $3.25) 26 [Published 20 August 1968

Introduction

When lasers were first developed emphasis was placed on photoelectric beat techniques for studying the output spectra. In the few applications where resolving powers of 10^{10} to 10^{13} are really necessary (for gas laser experiments), these homodyning and heterodyning methods are, at the moment, the only available ones. With giant pulse lasers where, because of the short coherence times, resolving powers of 10^7 to 10^8 are adequate, it is found that these beat techniques alone are not reliable (Bradley, Engwell, McCullough, Magyar & Richardson 1968, following paper) and multiple-beam interferograms (Bradley, De Silva, Evans & Forrest 1963) play the most important role in evaluating the complex output spectra. A resolving power of 5×10^7, corresponding to a resolution limit of 10 MHz, necessary to resolve the transverse mode structure of giant pulse ruby lasers (Bradley, Engwell, McCullough, Magyar & Richardson 1966), requires a plane Fabry–Pérot interferometer separation of 40 cm, assuming an instrumental finesse of 40. (A laser pulse halfwidth greater than 50 ns would be required to achieve this resolution limit.) Apart from the practical difficulties of alining a 40 cm gap plane etalon and keeping it in adjustment to the accuracy required to achieve such a high finesse, any spectral variations across the laser wavefront are integrated in the recorded interferogram, since the plane interferometer is translationally invariant in a parallel beam. Likewise no information is obtained on the spatial coherence of the source. It was these considerations which led us to consider the use of the spherical Fabry–Pérot etalon for giant pulse spectrography.

Spherical Fabry–Pérot interferograms

The photoelectric spherical Fabry–Pérot, time sequential scanning spectrometer is widely used for examining continuous wave lasers (Fork, Herriott & Kogelnik 1964) and has been employed with atomic beam sources (Jackson 1961). With short-duration laser giant pulses the spectral resolution limit, set by the temporal coherence of the source itself, cannot be achieved with this device (Bradley, Bates, Juulman & Majumdar 1964). Spherical Fabry–Pérot etalons, with the spherical mirrors separated by exactly their radius of curvature, have been employed with image tube detection, for time-resolved spectroscopy of ruby laser relaxation oscillations (Hanes & Stoicheff 1962). When the instrument is illuminated by a parallel laser beam (or other highly monochromatic parallel beam) a fringe pattern of concentric rings is obtained. These fringes are the spherical aberration pattern of the mirrors sharpened by multiple reflexion and are only visible when the etalon is illuminated by a monochromatic axial point source or its equivalent laser wavefront. Such spherical interferograms are not very suitable for producing simultaneously a spectrum extending over several orders of the free spectral range, as in the classical photographic use of the plane Fabry–Pérot interferometer. This is because when the mirrors are separated by exactly their radius of curvature, as in the original confocal instrument (Connes 1958), the order of interference of the resulting fringe pattern decreases as the fourth power of the fringe radius, compared with the square law dependence in the case of the plane interferometer. It is well known (Zernike 1948; Nienhius 1948; Bradley 1962) that the spherical aberration diffraction patterns of optical elements are radically altered by the addition of a defocusing term. Thus if the confocal

interferometer is slightly defocused by reducing the mirror separation by the appropriate amount, the resulting fringe pattern has a nearly linear wavenumber dispersion over a considerable annular region outside the central axial fringe.

Simple optical path difference calculation

The structure of the interference fringe pattern for a particular mirror separation is most easily calculated by considering the optical path difference between successively reflected rays as a function of the ray zonal radius. Figure 1 represents an incoming plane wavefront defined by the rays AB, CD, EF, passing through an interferometer, consisting of two high reflectivity spherical mirrors of equal radii of curvature, R, and separated by the distance

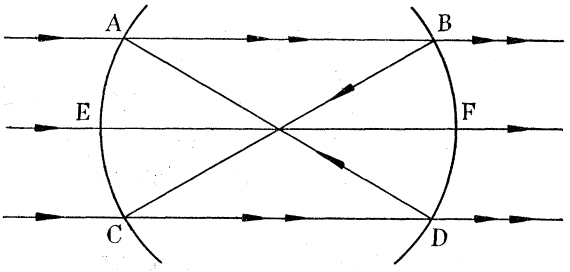

Figure 1. Ray paths, to a first approximation, through spherical mirror interferometer.

$EF = R+\rho$. AB and CD are both parallel to and distant r, the zonal radius, from the axial ray EF passing through the centres of curvature of the symmetrically arranged mirrors. ABCDAB represents, to a first approximation, the path of a double-pass ray (reflected successively at B, C, D and A) for which the condition for constructive interference is given by (Connes 1958; Jackson 1961),

$$4(R+\rho)-(r^4/R^3)-(4\rho r^2/R^2) = m\lambda. \tag{1}$$

The structure of the fringe pattern is determined by the value of ρ. The second term of (1) representing the spherical aberration, gives rise to the quartic fringes when $\rho = 0$. The third term is the defocusing term which varies as ρr^2. The equation is accurate to fifth-order terms in r/R and to first-order terms in $\rho r^2/R^3$.

By choosing a suitable small negative value for ρ, the aberration term can be made to dominate at the outside of the fringe pattern, while the defocusing term, of opposite sign, dominates for small values of the zonal radius r. A region of quasi-linear dispersion then exists in the annular region between the two regimes.

Defining a 'fringe number' $p(r)$ such that $p(r) = m_0-m(r)$, where $m(r)$ is the order of interference at zonal radius r, and m_0 is the order at the centre of the ring system, we obtain from (1) the relation

$$p\lambda = (r^4/R^3)+(4\rho r^2/R^2). \tag{2}$$

Then p is zero when $r = 0$ corresponding to the axial ray EF. For the non-confocal arrangement the fringe number is also zero, for negative values of ρ, when $r = (-4\rho R)^{\frac{1}{2}}$. Differentiation and rearrangement of (2) give $\mathrm{d}^2\lambda/\mathrm{d}r^2 = 0$, and $\mathrm{d}\lambda/\mathrm{d}r =$ constant for

$$r^2+\tfrac{2}{3}\rho R = 0. \tag{3}$$

Choosing a negative value of ρ to satisfy relation (3) a linear wavenumber dispersion with zonal radius and hence with fringe radius is obtained in the region of $r = (-2\rho R/3)^{\frac{1}{2}}$.

Figure 12, plate 1, shows how the fringe number p varies with the zonal radius for the two values $\rho = 0$ (confocal) and $\rho \simeq -200\ \mu$m (10 cm radii of curvature mirrors) and the type of fringes obtained in the two cases. The quasi-linear dispersion region is seen to occur in the neighbourhood of the point of inflexion in the curve of p against r. The interferograms were obtained with the use of a He—Ne gas laser in single mode operation. Because of drifting frequency the fringes are somewhat broader than the instrument profile.

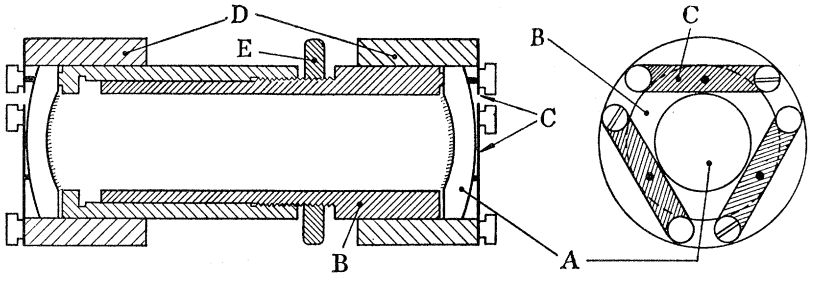

FIGURE 2. Sectional and end elevation of the etalon (not to scale) showing essential constructional details.

INSTRUMENT CONSTRUCTION

Figure 2 (not to scale) shows the essential details of the construction of the interferometers at present in use in our laboratories.

The plates (A) of the instrument are of optical grade fused silica, and are $1\frac{1}{2}$ in. diameter by approximately $\frac{3}{8}$ in. thick. The inner face of each plate has a 1 in. aperture, concave spherical surface of the appropriate radius of curvature (usually 5, 10 or 20 cm). These surfaces are polished identically spherical to $\lambda/75$ (in the green) over the central 0·5 cm diameter region, and are coated with either multilayer dielectric or protected silver reflecting coatings, of reflectivity in the range 0·95 to 0·98 at the relevant wavelength. The outer surfaces of the plates (plane in earlier versions of the instrument) are also spherical as indicated in the diagram. The radius of this curvature is chosen to correct for the divergence of the inner mirror surface. This is necessary to avoid deterioration of the fringe finesse (see below).

The spacer (B) is a hollow cylinder of invar steel of $1\frac{1}{2}$ in. outer diameter and 1 in. inner diameter. The plane shoulders of the mirrors rest against three 1 mm square raised flats located at intervals of 120° round each of the annular ends. The two surfaces defined by these sets of flats are plane and parallel to better than 5′. The spacer is made in two parts as shown, so that its length is continuously variable by means of the 40 T.P.I. screw and thread adjustment. When in use, the length of the spacer is such that the pole separation of the mirrors is a few hundred microns (the value of ρ above) less than the radius of curvature of the reflecting surfaces. The distance is then fixed by means of the locking ring (E).

Each plate is held in position by three spring strips (C), which bear on the outer surface of the plate directly opposite the spacer flats. This method of locating the mirrors avoids distortion of their surfaces. The springs are mounted on collars (D) closely fitted over the ends of the invar spacer. The assembled instrument is held by the threaded end of the spacer in an optical mount permitting adjustment of the orientation of its axis and lateral

displacement in a horizontal plane. The mount has a circular scale indicating the value of ρ. Once set for the correct separation the interferometer remains in perfect adjustment permanently and is not affected by vibration.

Computation of fringe profiles by wavefront tracing

The simple optical path calculation outlined above is adequate for determining the positions of the fringes and the location of the quasi-linear dispersion region. However, it gives no information about the fringe profiles, finesse, or optimum conditions of use of the defocused spherical Fabry–Pérot interferometer (hereafter designated DFPS). We have therefore computed on an ICT 1905 the wavefronts of the defocused spherical etalon by repetitive numerical tracing of the wavenormals.

The following experimental arrangements were considered.

(i) One half of the input beam is blocked off by a straight edge. This eliminates interference effects between portions of the beam which enter the DFPS at points which are diametrically opposite with respect to the instrumental axis. The computed results also hold for unobstructed spatially incoherent beams.

(ii) An unobstructed input beam of high spatial coherence.

(iii) An interferometer in which the blocking off is accomplished by making half of each of the spherical mirrors totally reflecting, as in the original instrument of Connes (1958).

(i) *Semi-circular input aperture*

The progressive distortion of an incident plane wavefront after 4, 8, 12, 16 and 20 passes through a DFPS with $R = 10$ cm and $\rho = -200\,\mu$m is shown in figure 3 and the fringe profiles obtained by summing the wavefronts from 45 passes for a mirror reflectivity of 0·95 and a wavelength of 7000 Å are shown in figure 4.

The fringe intensity is given relative to I_0 the peak intensity of the fringe at the centre of the pattern where $p = 0$. In the calculation it was assumed that m_0, the order of interference at the centre, was an integer. Physically this is equivalent to very slight wavenumber tuning of maximum amount 0·025 cm^{-1}. Since there are four reflexions for each double pass of the spherical etalon, $\mathscr{R}^2$ replaces $\mathscr{R}$ in the Airy sum and $I_0 = (1-\mathscr{R})^2/(1-\mathscr{R}^2)^2$. For high reflectivity $\mathscr{R}$, I_0 is approximately one quarter of the input intensity. Absorption was assumed to be negligible in all calculations. This is a reasonable assumption for good dielectric mirrors.

For comparison purposes the fringe number p, as given by relation (2) above, is plotted as a function of zonal radius on the same abscissa scale in figure 4. Excellent agreement with the computed fringe positions is evident.

Figure 5 shows in more detail the lower portions of the first and second fringes out from the centre ($p = -1$ and -2 respectively) together with the intervening region. The computed contrast C of 4×10^2 is the value to be expected from the Airy formula calculation (Tolansky 1947) when $\mathscr{R}^2$ is substituted for $\mathscr{R}$,

$$C = (1+\mathscr{R}^2)^2/(1-\mathscr{R}^2)^2 \quad \text{for} \quad \mathscr{R} = 0{\cdot}95.$$

To a first approximation, successive rays through the interferometer, shown as broken lines in figure 6, are coincident and intersect at the midpoint C of its axis. Ideally then the

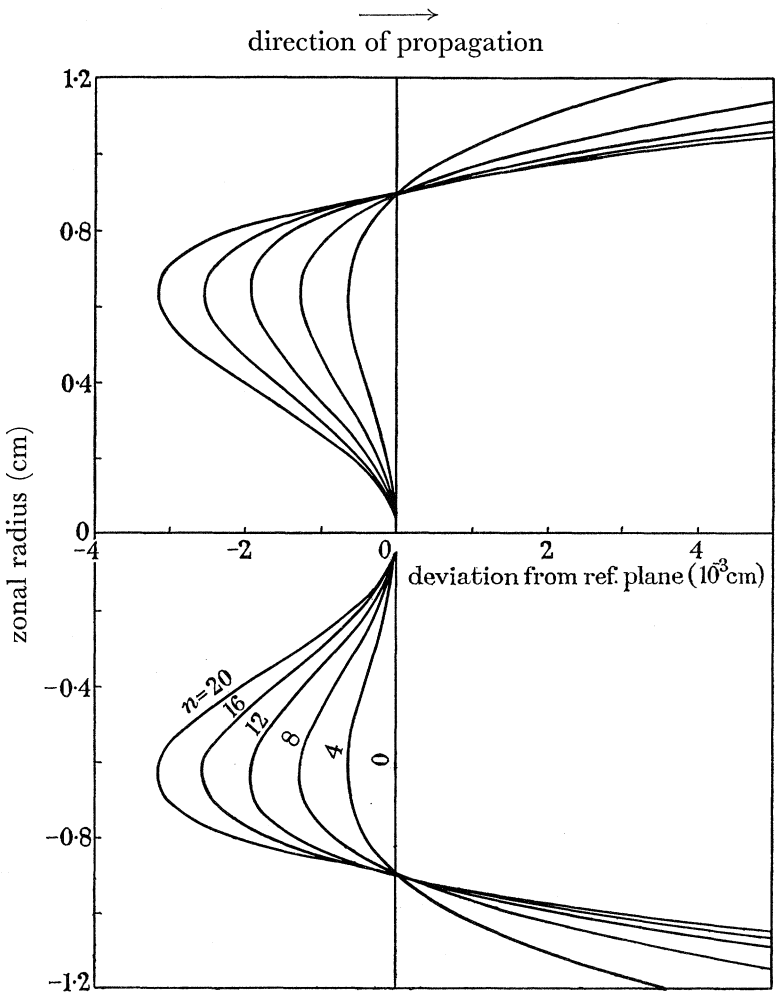

FIGURE 3. Progressive distortion of the wavefront after n passes through the defocused etalon.

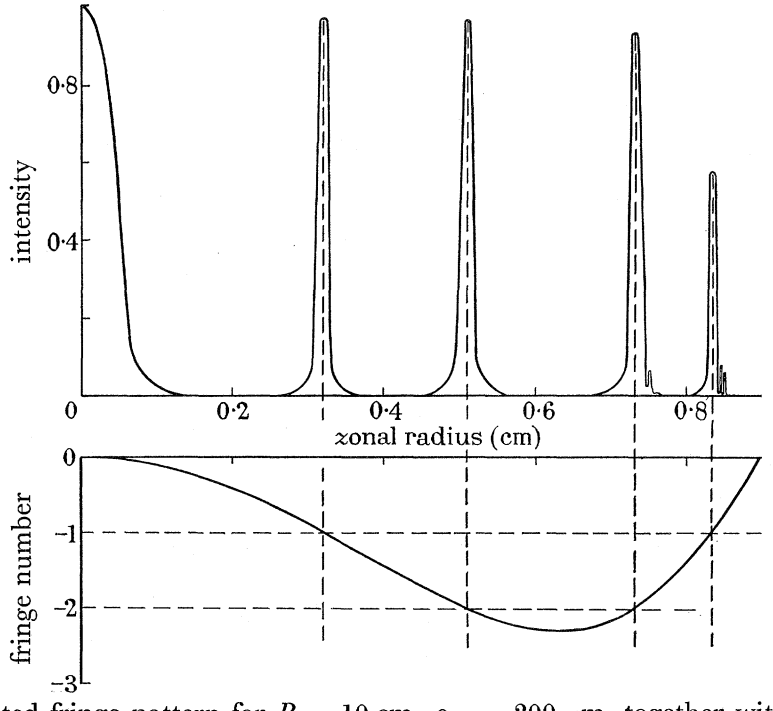

FIGURE 4. Computed fringe pattern for $R = 10$ cm, $\rho = -200$ μm, together with a plot of fringe number p as a function of zonal radius calculated from equation (2).

fringe system is not localized and may be obtained by summing the wavefronts on any plane perpendicular to the axis. In fact, however, the rays are not exactly coincident, and follow the paths shown by the solid lines of figure 6.

The effect is exaggerated in the figure, which is not to scale. The best image of the rings is obtained by focusing on the plane where the interfering rays intersect since the fringes are localized here. This position is in the vicinity of the equatorial plane of the instrument.

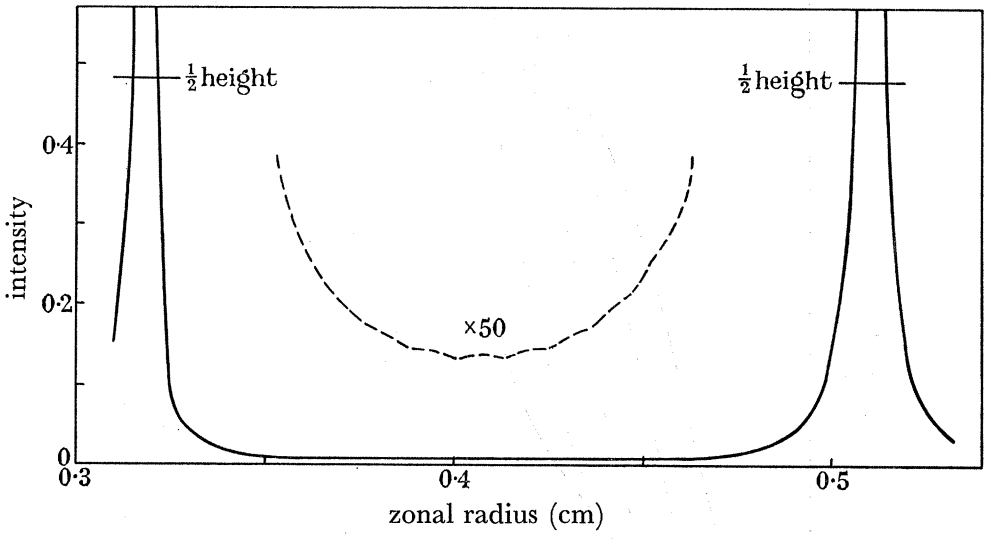

FIGURE 5. Computed intensity distribution showing the lower portions of first two fringes and the intervening region. Same etalon parameters as figure 4.

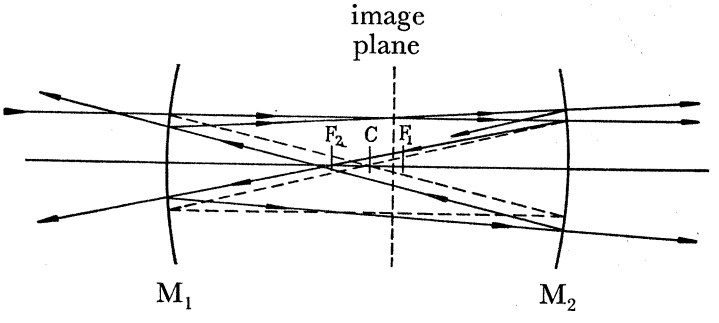

FIGURE 6. Exact ray paths through the etalon, showing effect of the defocusing term. (Not to scale.)

Although the deviation from coincidence of the rays is rather small, correct focusing is necessary to obtain optimum fringe finesse. This is illustrated by figure 7 showing the computed profile of the $p = -1$ fringe under the same conditions as before ($R = 10$ cm, $\rho = -200$ μm, $\lambda = 7000$ Å, $\mathscr{R} = 0{\cdot}95$), at planes 5·0, 5·25, 5·5, 5·75 and 6·0 cm respectively from the input mirror. It can be seen that the best fringe profile is obtained if the camera is focused on a plane about 5·9 cm from the input mirror. Under these conditions the finesse (defined as the value of $\mathrm{d}r/\mathrm{d}p$ at the fringe position divided by the fringe width at half maximum intensity) is 30·5. This value is practically the same as the reflexion finesse for a plane Fabry–Pérot interferometer (hereafter designated FPP) of equivalent reflectivity 0·9025 (the square of the 0·95 reflectivity of the DFPS).

Figure 8 compares the DFPS fringe for optimum conditions, i.e. computed at a plane 5·9 cm from the input mirror, with the equivalent Airy fringe profile adjusted to the same peak height and for the same fringe separation. The half-height widths of the two curves are essentially the same, and the DFPS profile follows that of the Airy curve closely except in the wings.

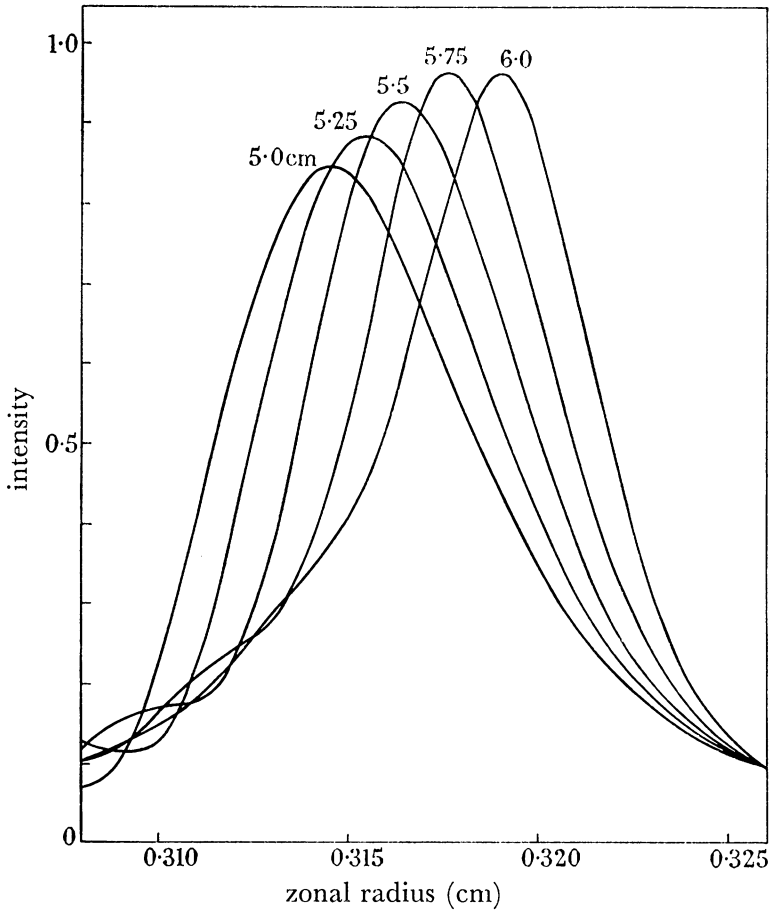

FIGURE 7. Computed effect on fringe profile of focusing on a plane located at various distances from the input mirror. First fringe from centre, $p = -1$.

Although the finesse of the DFPS and that of the equivalent FPP are almost equal under these conditions, for reflectivities greater than 0·95 the finesse of the DFPS does not increase as rapidly with reflectivity as does the reflexion finesse of the FPP. The solid curve, DFPS (1) of figure 9 shows the reflexion finesse of the DFPS, for experimental arrangement (i), as a function of the reflectivity, $\mathscr{R}$, compared with that of an FPP of equivalent reflectivity $\mathscr{R}^2$ (curve FPP (1)). The DFPS (1) curve resembles that of a Lummer–Gehrcke interferometer (Born & Wolf 1965). This is to be expected since there is a reduction in the effective number of interfering beams, due to the failure of the rays to continue to pass through the image plane at precisely the same point.

A further feature of interest is the appearance of secondary maxima, the intensity of which increases relative to that of the main peak as the reflectivity is increased. These secondary fringes, seen in the outer fringes of figure 4, closely resemble those obtained in a wedge etalon (Hermansen 1959) when the wedge angle is too large in relation to the number

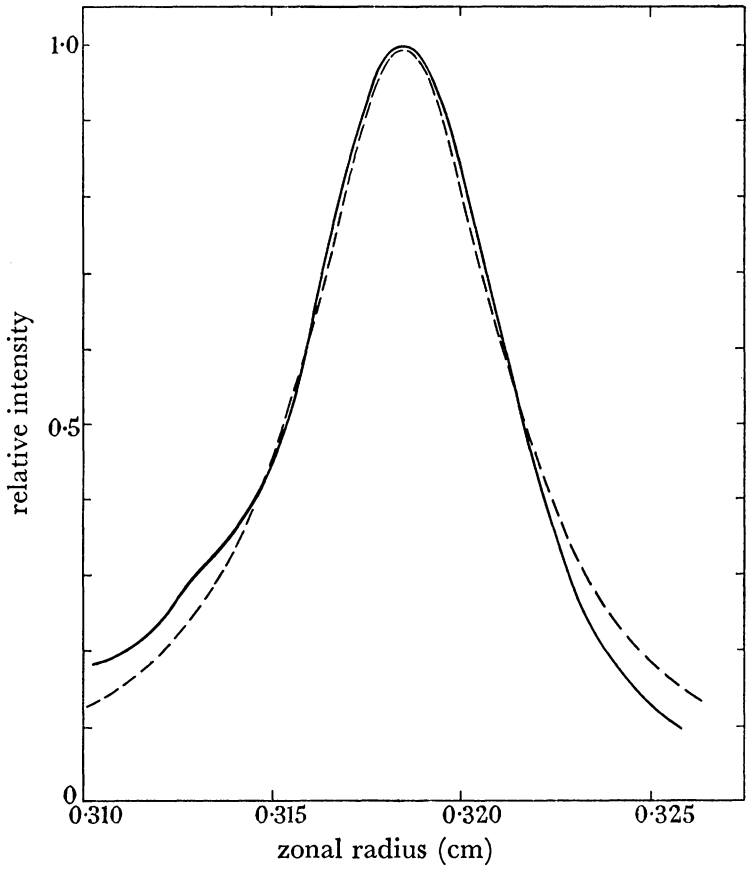

FIGURE 8. Comparison between an optimized DFPS ring profile (computed) (——) and the Airy curve (— — —) for the square of the reflectivity and for the same peak intensity and fringe separation. Finesse = 30·5 for both curves.

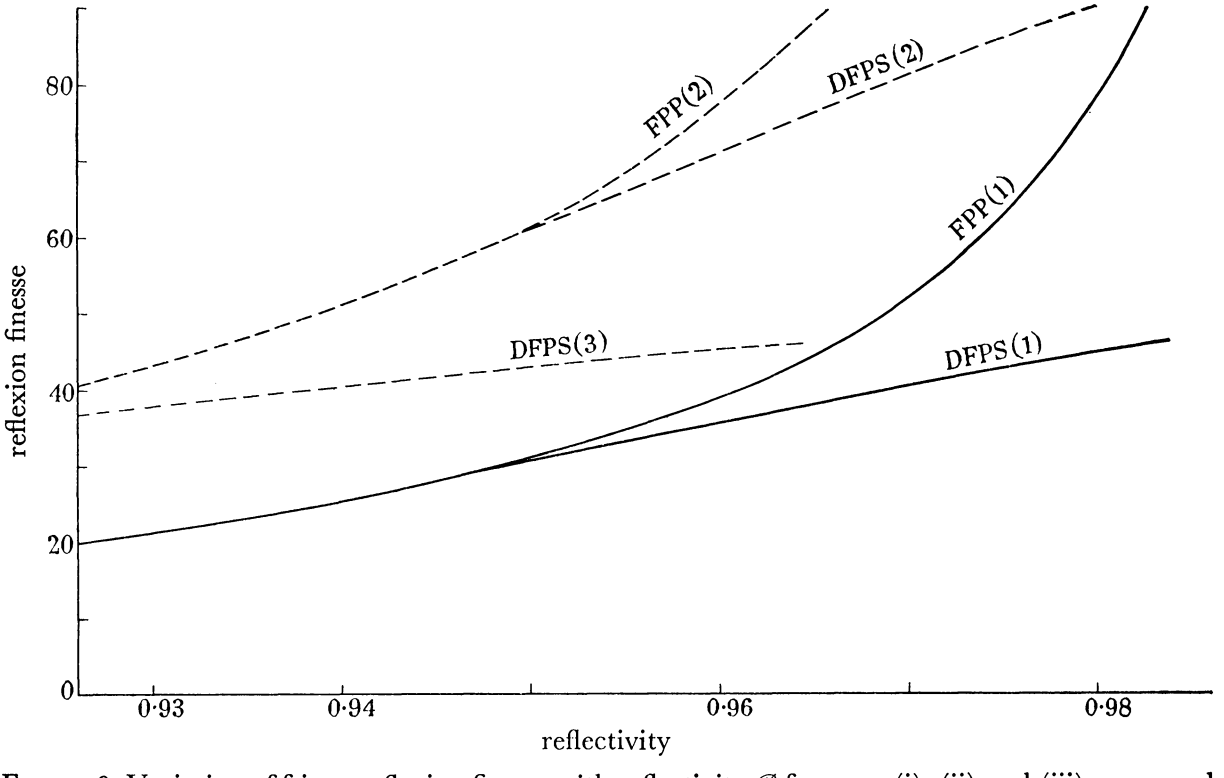

FIGURE 9. Variation of fringe reflexion finesse with reflectivity $\mathscr{R}$ for cases (i), (ii) and (iii) compared with variation of reflexion finesse of a FPP of equivalent reflectivity.

of effective passes (Brossel 1947; Tolansky 1948). In the case of the DFPS the wedge angle arises from the relative inclination of the straight through and reflected wavefronts. Owing to the spherical aberration of the mirrors this angle increases with zonal radius. However, these secondary maxima only become important for very high reflectivities and for large values of the zonal radius. Normally they do not occur in the linear dispersion zone.

In all the above computations we assumed that the input plane wave was not distorted by the first mirror substrate. In our earlier instruments, however, the input plate was an effective plano-concave lens which, in the case of a 10 cm etalon, had a focal length of approximately 20 cm. A plane wavefront incident upon the DFPS then becomes a diverging spherical wavefront centred on an effective axial point source some 20 cm on the input side of the instrument. The effect of this lens was also investigated on the computer. When the effective point source is 25 cm from the equatorial plane of the DFPS (i.e. 20 cm from the input mirror) the fringe width is increased by nearly 60 % and, more seriously, the profile is distorted. The fringe profile and finesse are restored when the effective point source is at infinity, i.e. in the absence of the lens effect. Even partial correction produces a noticeable improvement. For best results it is necessary to correct the diverging lens either by employing a converging correcting lens, or by appropriate curvature of the front surface of the input plate.

(ii) *Full input aperture; measurement of spatial coherence*

When a DFPS is accurately alined normal to a laser beam of high spatial coherence, an alternation in intensity of successive rings can be clearly observed. Every second ring disappears or becomes very faint. This effect is due to interference between corresponding regions of the incident wavefront which enter the interferometer at points which are diametrically opposite relative to the instrument axis. Consideration of figure 6 shows that a light ray entering the DFPS, after two reflexions, travels (to good approximation) along the path of a ray entering at a diametrically opposite point. With a spatially coherent input beam interference results. If the interferometer optical path difference for this value of the zonal radius is an odd integral number of wavelengths this two beam interference will be destructive. For an even integer, constructive interference will occur. Consequently the multiple beam fringes of even order will be quadrupled in intensity while those of odd order disappear. When the input beam is not completely spatially coherent the visibility of this intensity alternation gives a direct measure of how the degree of spatial coherence (Born & Wolf 1965) of the laser wavefront varies with beam aperture.

In addition to the increase in intensity of the even-order rings, the effective fringe finesse is doubled. This is because, to the set of rays with amplitudes progressing as $1, \mathscr{R}^2, \mathscr{R}^4, \ldots$ (where the amplitude coefficient of reflexion is $\mathscr{R}^{\frac{1}{2}}$), there is added a second set also in phase and with amplitudes $\mathscr{R}, \mathscr{R}^3, \mathscr{R}^5, \ldots$. In this case there is no increase in the aberration, and for values of $\mathscr{R}$ greater than 0·9 the effective finesse is increased by a factor very close to two. The broken line DFPS (2) of figure 9 then shows the dependence of finesse on reflectivity, compared with the FPP reflexion finesse for the same reflectivity (curve FPP (2)). We retain the same definition of finesse, that is $|\mathrm{d}r/\mathrm{d}p|$ divided by the half-height width. This twofold increase in effective finesse depends on the complete disappearance of the odd-order fringes, and consequent doubling of the free

spectral range. In practice these fringes usually remain faintly visible as a result of imperfections in mirrors, alinement or spatial coherence.

When the DFPS, used in this way, is not correctly alined normal to the input beam, instead of the intensity alternation of the fringes, a set of almost straight two-beam interference fringes is superposed on the ring pattern. These also arise from interference between opposite points on the coherence wavefront. As the alinement is improved, the two-beam fringes are seen to broaden and eventually change into a set of circular fringes, located so that they block out every alternate ring of the multiple beam interferogram, to produce the intensity alternation referred to above. These initially straight two-beam fringes provide an easy and convenient method of correctly alining the instrument with a gas laser beam. When a straight edge is inserted to cut off slightly less than half of the input beam, a uniform intensity interferogram is obtained over most of the field of view, apart from a central strip in which the intensity alternation (and, when the interferometer is not exactly alined, the two-beam straight fringes) can be observed. This configuration provides information on spatial coherence while retaining the coherence-independent finesse in the main part of the interferogram. The result is illustrated in figure 13*a*, plate 2, obtained with a He—Ne laser operating on three longitudinal modes. It can clearly be seen that if the central frequency mode is symmetric then the other two are antisymmetric and vice versa since if the phase of a transverse mode is antisymmetric, it is the odd-order rings which are intensified instead of the even-order rings.

When a half of each of the mirrors is totally reflecting (case (iii) above) no interference can take place between opposite sides of the input. However, the amplitudes are now attenuated by $\mathscr{R}$, not $\mathscr{R}^2$, on each pass, so the system is equivalent to that of case (i) with plate reflectivity $\mathscr{R}^{\frac{1}{2}}$ instead of $\mathscr{R}$. However, there is an increase in aberration effects associated with such a change in reflectivity (increase in secondary maxima, etc.), and consequently the finesse is increased in this case by a factor appreciably less than 2. The computed curve DFPS (3) is shown broken in figure 9. With this form of the instrument, of course, only half of the ring system is visible and there is no information on spatial coherence.

Design of a defocused spherical interferometer for laser spectroscopy

In designing a DFPS for operation at a given wavelength and under specified conditions, the parameters to be considered are the value of the radius of curvature R, the deviation, ρ, of the plate separation from this value, and the reflectivity $\mathscr{R}$ of the plates. As we have seen, the value of the reflectivity is not critical, but there is little point in exceeding $\mathscr{R} = 0{\cdot}97$ because of the disproportionately small gain in the finesse and the accentuation of the wedge-etalon type subsidiary maxima.

In deciding the values of R and ρ, the following points must be considered. Since we require for linear wavenumber dispersion that $r = (-\frac{2}{3}\rho R)^{\frac{1}{2}}$, for a given value of R the zonal radius r of the linear dispersion region is proportional to $|\rho|^{\frac{1}{2}}$. Hence if $|\rho|$ is too large the finesse at the linear region falls off due to asymmetry of the fringe profile and the associated secondary maxima as described above. If, however, ρ and R are increased in the same proportion, then although r also increases, the finesse remains practically unchanged because the reduced curvature leads to a smaller effective wedge angle. The small change

in finesse which does occur is due to the slight dependence of the finesse of wavelength. If in addition the wavelength also were increased in proportion to ρ and R, then the change in finesse would be zero owing to the proportionate scaling of all parameters. The wavelength dependence of the finesse is in any case rather small, varying in a typical case by a factor of 1·2 for a wavelength change by a factor of 5. Thus it may be neglected when visible or near-visible radiation is considered. The finesse at the linear dispersion region then depends only on the reflectivity, $\mathscr{R}$, and on the factor ρ/R. This is illustrated by the broken curves of figure 10 drawn through computed values of the finesse at linearity for experimental arrangement (i), for various values of ρ/R for fixed $\mathscr{R}$.

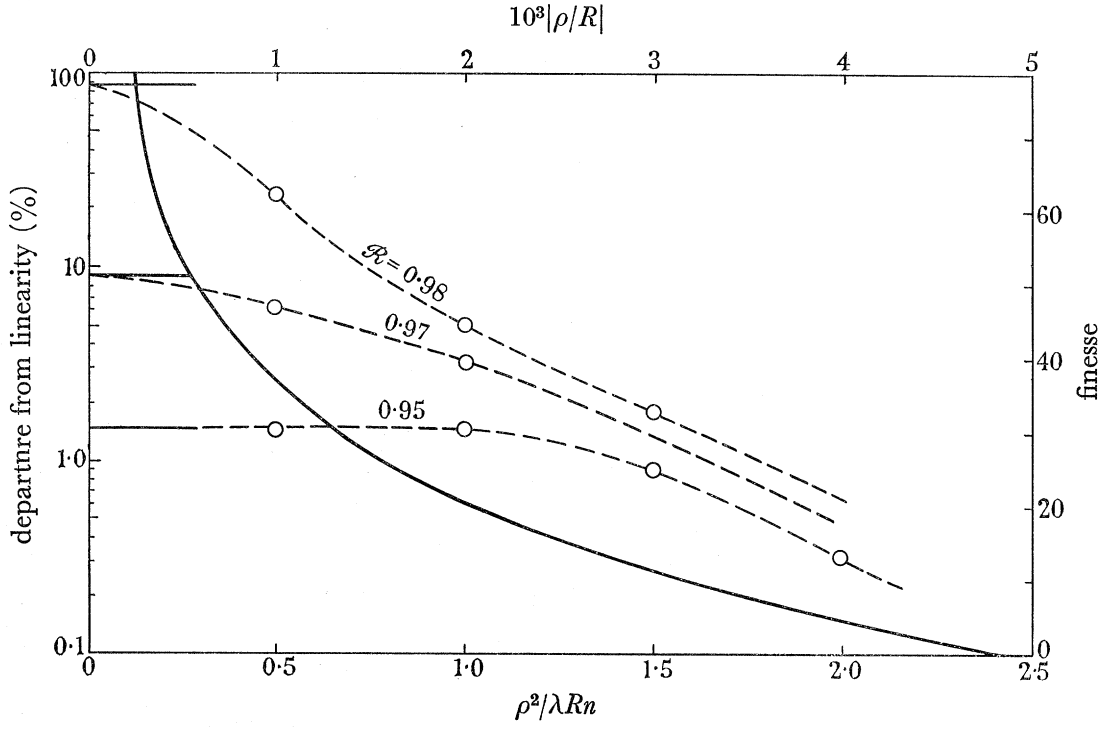

FIGURE 10. Percentage departure from linearity (solid curve), for experimental arrangement (i), at outer edge of quasi-linear region as a function of $\rho^2/\lambda Rn$, where n is the number of free spectral ranges in the region. Broken curves—optimum finesse at linearity as a function of ρ/R for various reflectivities. Horizontal solid lines on left indicate the Airy finesse for the equivalent reflectivity $\mathscr{R}^2$. Circles represent computed values.

It is clear that for maximum finesse at linearity a small value of ρ/R is desirable. However, from equation (2) it is easily shown that the departure from linearity, as a function of distance from the point of inflexion on the fringe number—zonal radius curve (figure 12, plate 1), depends on the value of the parameter $\rho^2/\lambda R$, and becomes unacceptably high for small values of this factor. The solid curve of figure 10 shows the dependence of the departure from linearity on the factor $\rho^2/\lambda Rn$, where n is the number of free spectral ranges required within the quasi-linear region. (The departure from linearity is approximately the same for $\frac{1}{2}n$ free spectral ranges in either direction, but the value plotted is the higher of the two values.)

An example may help to clarify the above. Suppose that an etalon with $R = 10$ cm is to be used at 7000 Å, with the requirements that there should be two free spectral ranges

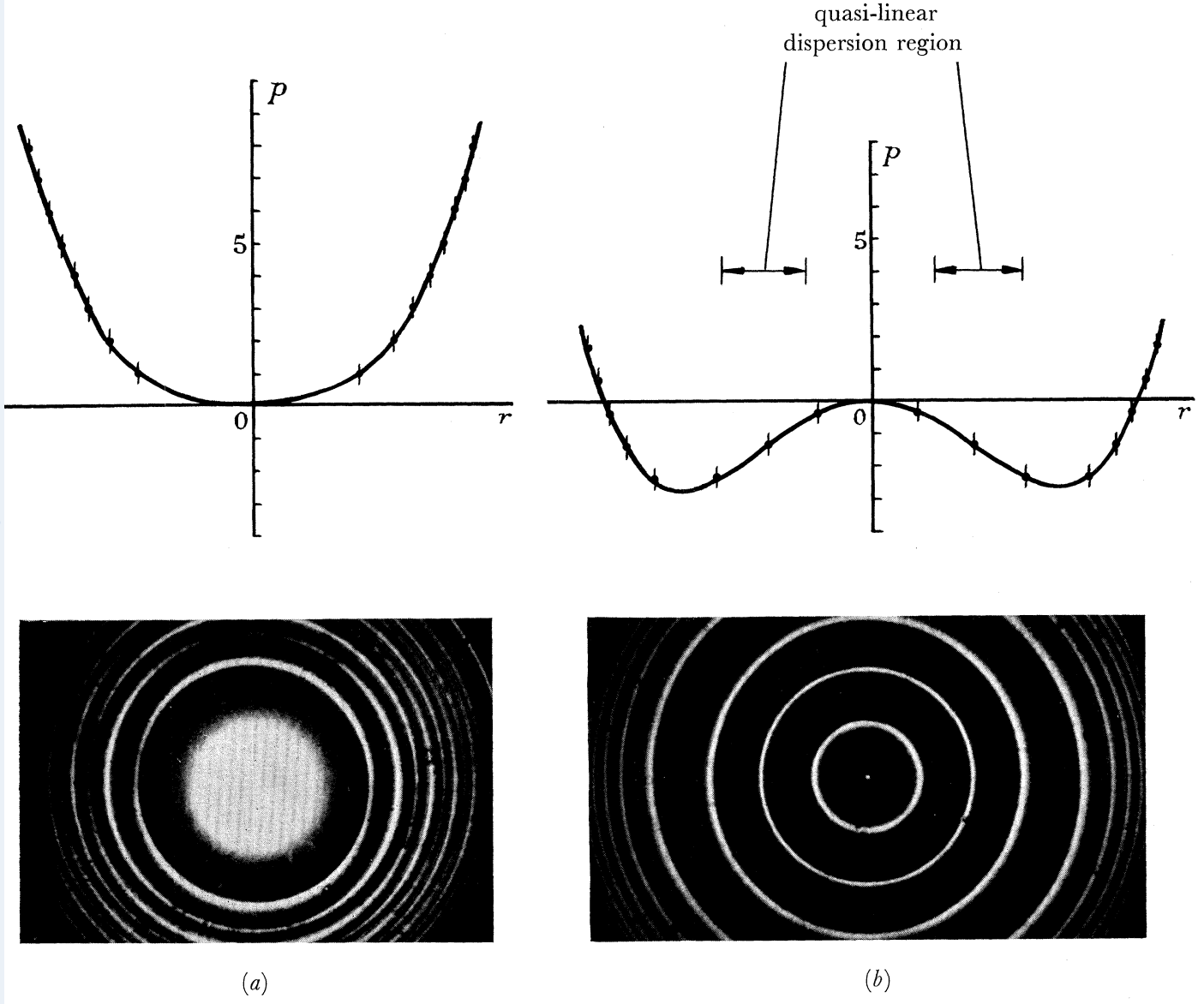

(*a*) (*b*)

FIGURE 12. Dependence of fringe number, p, on the zonal radius, r, for (*a*) confocal spherical interferometer, $\rho = 0$ and (*b*) defocused spherical interferometer, $\rho = -200$ μm, and the corresponding He—Ne single mode gas laser interferograms.

(*Facing p.* 220)

PHILOSOPHICAL TRANSACTIONS OF THE ROYAL SOCIETY A MATHEMATICAL, PHYSICAL & ENGINEERING SCIENCES

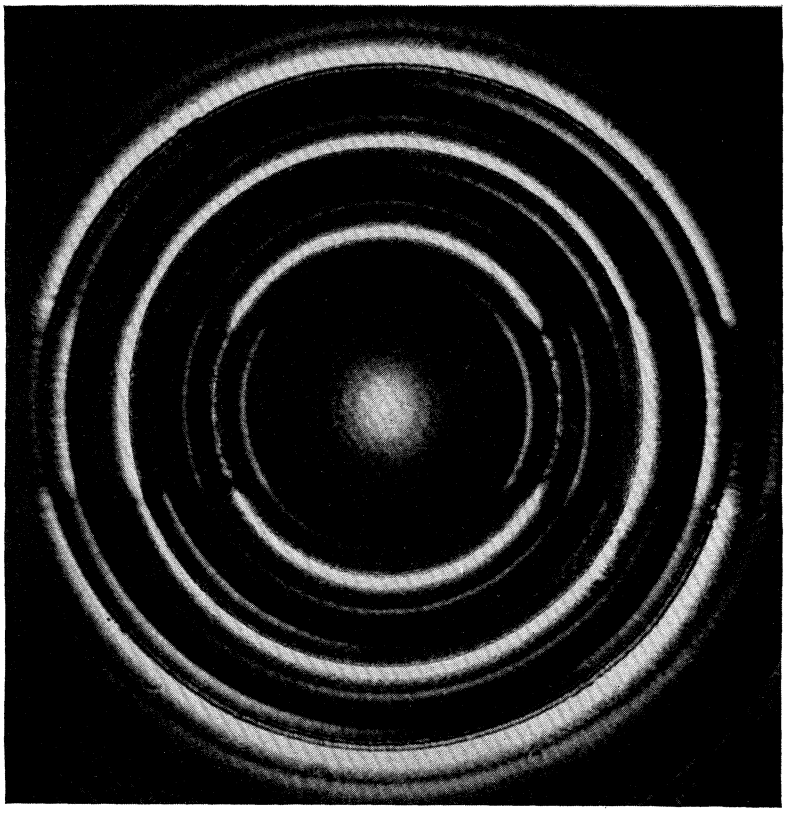

(*a*)

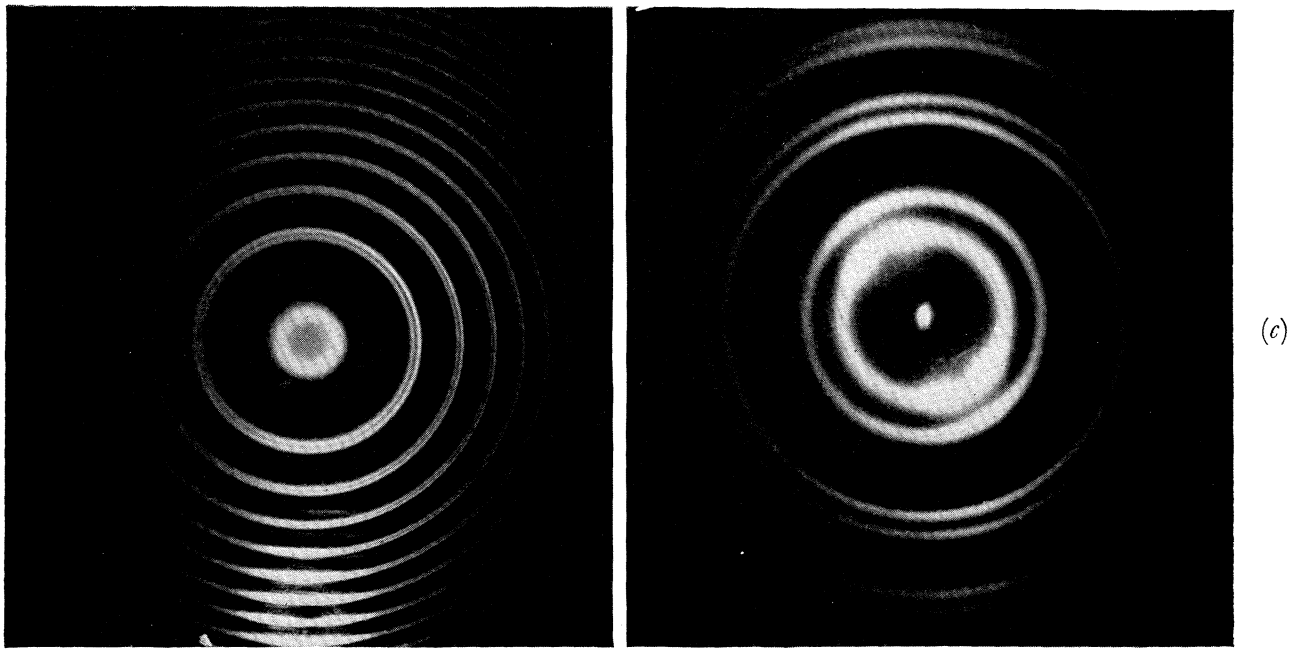

(*b*) (*c*)

FIGURE 13. (*a*) Effect of blocking off a segment of the interferometer input aperture. Interferogram of gas laser operating on three longitudinal modes showing alternation in fringe intensities along diametral section due to spatial coherence of the laser modes.
(*b*), (*c*) Simultaneous interferograms of two longitudinal modes of a gas laser taken with 10 cm gap (*b*) plane and (*c*) defocused spherical mirror etalons respectively.

PHILOSOPHICAL TRANSACTIONS OF THE ROYAL SOCIETY A MATHEMATICAL, PHYSICAL & ENGINEERING SCIENCES

in the region of quasi-linear dispersion, that the departure from linearity should not exceed 2 % at the edges of this region, and that a finesse of 25 or better is needed. For mirrors of reflectivity 0·95, the restriction on the finesse means, from figure 10, that $|\rho/R|$ must be less than $3{\cdot}0\times10^{-3}$, or $|\rho| < 3{\cdot}0\times10^{-2}$ cm. For this value of $|\rho/R|$ and putting $n = 2$, we obtain $\rho^2/\lambda Rn \leqslant 0{\cdot}64$. From the figure, the resulting maximum departure from linearity at the edge of the quasi-linear region is about 1·5 %. Alternatively, from the restriction on the linearity, we obtain the condition $\rho^2/\lambda Rn > 0{\cdot}55$, i.e. $|\rho| > 2{\cdot}8\times10^{-2}$ cm, which leads to a finesse of around 27. Thus in this case a value of $|\rho|$ between 280 and 300 μm is required to satisfy the specifications. The same design considerations apply to the three experimental arrangements above. Only the reflexion finesse obtained for a particular value of mirror reflectivity, $\mathscr{R}$, is different, as already discussed.

Since the input beam diameter must be large enough to include the quasi-linear annular region, and should not, for efficient illumination, be larger than this, some telescopic magnification or demagnification of the input beam may be necessary.

Discussion: Advantages of a defocused spherical interferometer for laser diagnostic spectroscopy

For comparison purposes figures 13*b*, *c*, plate 2, show simultaneous interferograms of two longitudinal modes of a gas laser taken with 10 cm gap (*b*) plane and (*c*) defocused spherical mirror etalons respectively. In both cases the recorded fringe finesse is limited

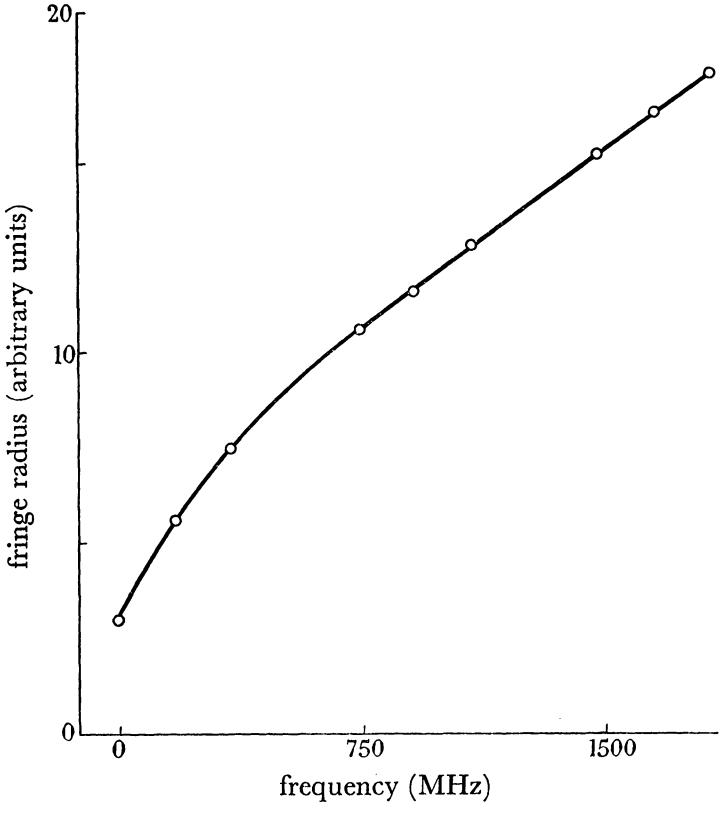

Figure 11. Frequency dispersion calibration curve of 10 cm defocused spherical interferometer derived from gas laser interferogram. Circles denote radial positions of the three laser longitudinal modes.

by fluctuations of the unstabilized gas laser frequency during the exposure of several seconds. The advantage of the quasi-linear dispersion of the spherical etalon is immediately apparent and it should be remembered that the resolving power is twice as great, assuming the same fringe finesse.

The frequency dispersion calibration curve of figure 11 was obtained from microdensitometer traces of an etalon interferogram obtained when three longitudinal modes of the gas laser are operating simultaneously. As can be seen, linearity is, in fact, largely preserved over a spectral spread considerably greater than the free spectral range of the 10 cm interferometer (750 MHz). With such linearity of dispersion, matching of the interferogram to the spatial resolution of the detector, photographic plate or image tube (Bradley *et al.* 1964), is then straightforward, and, more importantly, quantitative interpretation of small frequency differences is possible.

For practical reasons a much higher illumination of the detector can be achieved with a DFPS than with a FPP. When a plane interferometer is placed in a pure single mode laser beam, typically 1 to 2 mm diameter, the beam spread is insufficient to illuminate more than one ring of the interference pattern. As an example for a 5 cm gap interferometer a beam spread of 5×10^{-3} rad is needed to produce two rings. If light is not to be lost it is then necessary to telescopically demagnify the beam aperture until the diffraction spread of the light is sufficient. For our example this would require demagnification to 0·1 mm aperture which would rapidly lead to damage of the mirror coatings because of the high energy density involved. Employing a gas laser we have found that the plane interferometer when used under these conditions does in fact have an illumination of the same order as the equivalent DFPS.

If mirror damage is to be avoided the FPP has to be employed in the converging beam mounting leading to a serious loss in illumination (Tolansky 1947). The spherical interferometer can, of course, be used in a highly collimated beam of relatively wide aperture without a loss in illumination.

A further feature of the DFPS, important for laser spectroscopy, is that unlike the FPP it is not translationally invariant in a parallel laser beam. The interferogram provides information on any spectral variation across the wavefront which may be present. (With a plane interferometer this information could only be obtained by employing apertures and the whole beam cross-section could not be studied at once.) This property has proved very useful in interpreting streaked interferograms showing a time dependent frequency shift (Bradley *et al.* 1966*b*, 1968) in the output spectrum of a giant pulse ruby laser.

Finally, the DFPS has the important advantage in practice that its plates are permanently in adjustment, being much less critical in their relative alinement than is the case with an FPP of equivalent resolving power. The instrumental finesse is then not limited by mirror alinement and in practice a very high value can be obtained with a single mode laser beam. Thus with mirrors of 0·98 reflectivity the maximum instrumental finesse of nearly 90 (curve DFPS (2) of figure 9), corresponding to a spectral resolution limit of < 10 MHz (free spectral range 750 MHz), was recorded with a low power ruby laser giant pulse (Bradley *et al.* 1966*a*). To achieve this finesse with a FPP would require mirrors smooth, plane and parallel to better than $\lambda/250$ over the laser beam aperture. The only preparation needed for use of the DFPS is the alinement of the instrument axially with the

input beam. This is easily carried out with the aid of a He—Ne laser and the two-beam fringes mentioned earlier.

Several defocused spherical Fabry–Pérot interferometers of various separations are now employed in this laboratory for spectral monitoring of neodymium and ruby giant pulse lasers (Bradley *et al.* 1968).

The authors take this opportunity to thank Dr W. T. Welford for advice and helpful discussion on wavefront computing. Thanks are also due to Mr R. Morrison who was responsible for continuing improvements in the mechanical design and construction of the various interferometers tested, and to Mr H. W. Yates for his advice on the construction of the mirror substrates. The interferograms of figure 13 *b* and *c*, plate 2 were photographed by Mr M. E. Engwell and the frequency calibration curve was derived by Mr A. Durrant.

One of us (C. J. M.) is supported by a Research Studentship of the Ministry of Education for Northern Ireland. Substantial assistance has been received from the Science Research Council, both for the purchase of equipment and for the provision of technical support.

References

Born, M. & Wolf, E. 1965 *Principles of optics* (3*rd ed.*), pp. 345, 346, 505, 506. Oxford, London, Edinburgh, New York, Frankfurt, Paris: Pergamon Press.

Bradley, D. J. 1962 *Optica Acta* **9**, 365.

Bradley, D. J., De Silva, A. W., Evans, D. E. & Forrest, M. J. 1963 *Nature, Lond.* **199**, 1281.

Bradley, D. J., Bates, B., Juulman, C. O. L. & Majumdar, S. 1964 *Appl. Opt.* **3**, 1461.

Bradley, D. J., Engwell, M. S., McCullough, A. W., Magyar, C. & Richardson, M. C. 1966*a* *Appl. Phys. Lett.* **9**, 150.

Bradley, D. J., Magyar, G. & Richardson, M. C. 1966*b* *Nature, Lond.* **212**, 63.

Bradley, D. J. 1967 *Nature, Lond.* **215**, 499.

Bradley, D. J., Engwell, M. S., McCullough, A. W., Magyar, G. & Richardson, M. C. 1968 *Phil. Trans.* A **263**, 225.

Brossel, J. 1947 *Proc. Phys. Soc.* **59**, 224.

Connes, P. 1958 *J. Phys. Radium, Paris* **19**, 262.

Fork, R. L., Herriott, D. R. & Kogelnik, H. 1964 *Appl. Opt.* **3**, 1471.

Hanes, G. R. & Stoicheff, B. P. 1962 *Nature, Lond.* **195**, 587.

Hermansen, A. 1959 Abstracts of Fifth Meeting and Conference of the International Commission for Optics (ICO) in Stockholm.

Jackson, D. A. 1961 *Proc. Roy. Soc.* A **263**, 298.

Nienhus, K. 1948 Thesis, University of Gröningen.

Tolansky, S. 1947 *High resolution spectroscopy*. London: Methuen and Co.

Tolansky, S. 1948 *Multiple beam interferometry of surfaces and films*. Oxford University Press.

Zernike, F. 1948 *Proc. Phys. Soc.* **61**, 158.

PHILOSOPHICAL TRANSACTIONS OF THE ROYAL SOCIETY A MATHEMATICAL, PHYSICAL & ENGINEERING SCIENCES

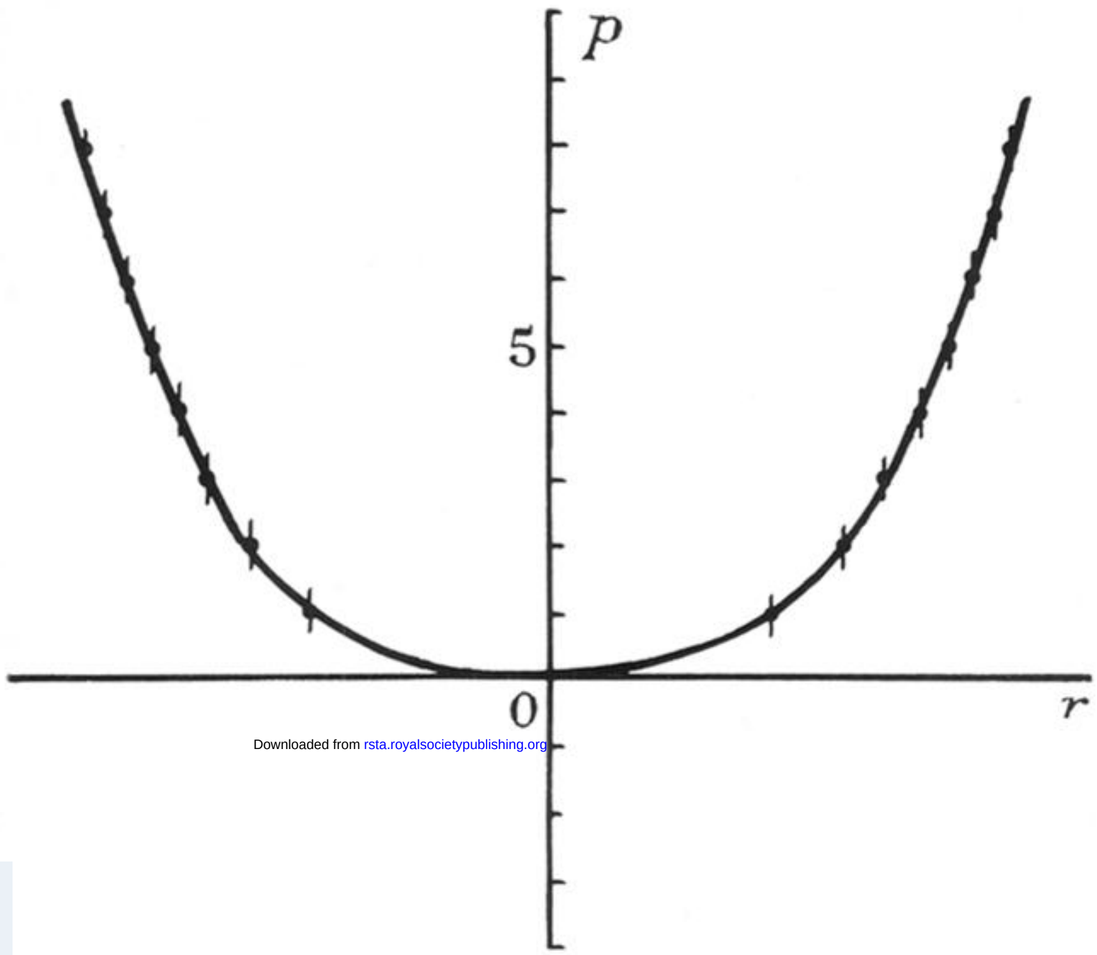

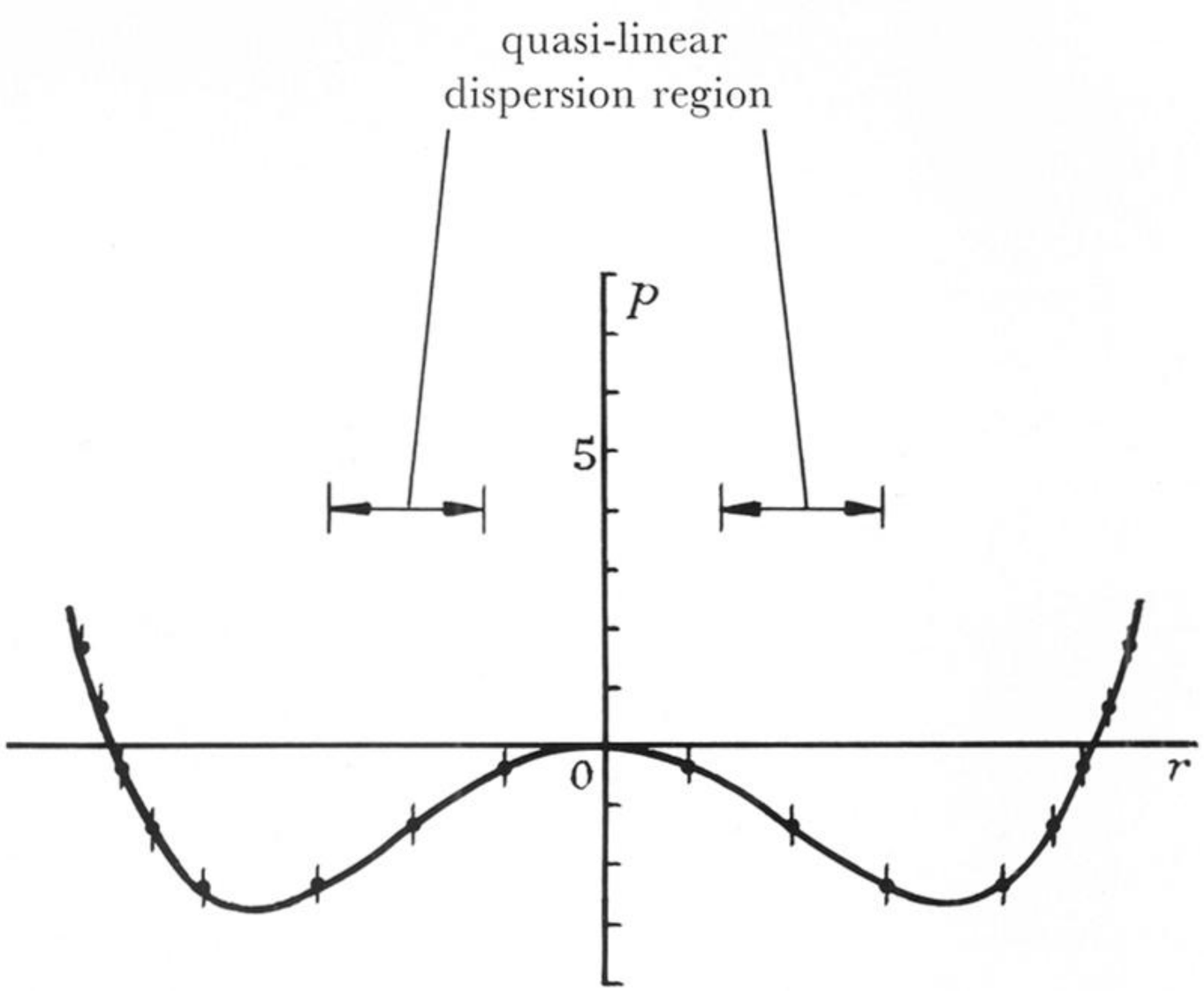

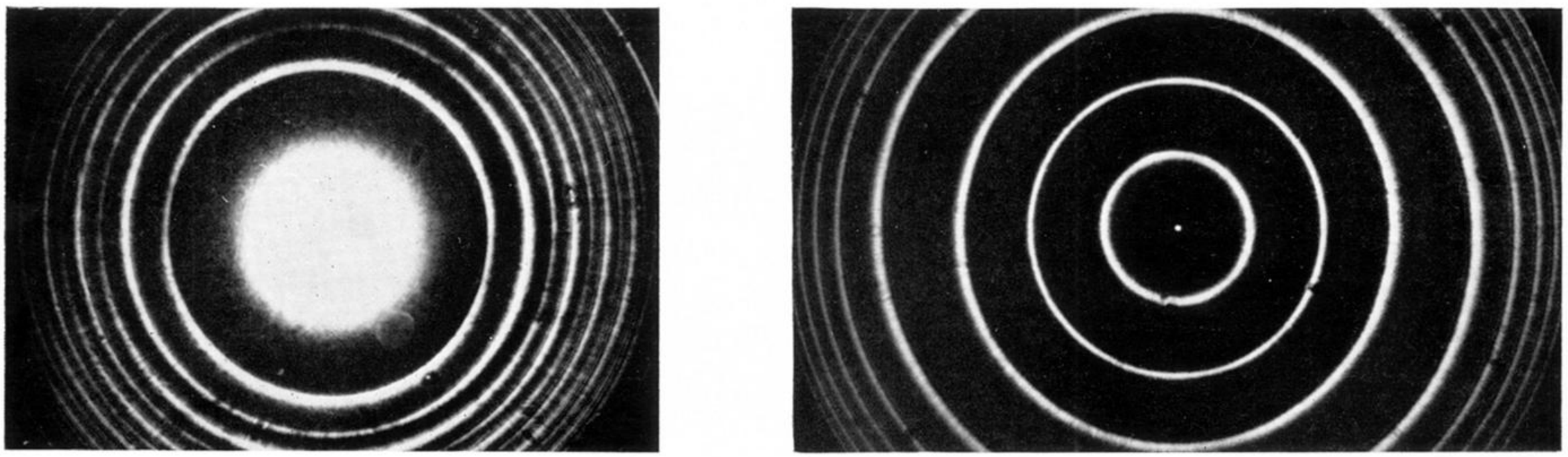

(*a*) (*b*)

FIGURE 12. Dependence of fringe number, p, on the zonal radius, r, for (*a*) confocal spherical interferometer, $\rho = 0$ and (*b*) defocused spherical interferometer, $\rho = -200\ \mu$m, and the corresponding He—Ne single mode gas laser interferograms.

PHILOSOPHICAL TRANSACTIONS OF THE ROYAL SOCIETY A MATHEMATICAL, PHYSICAL & ENGINEERING SCIENCES

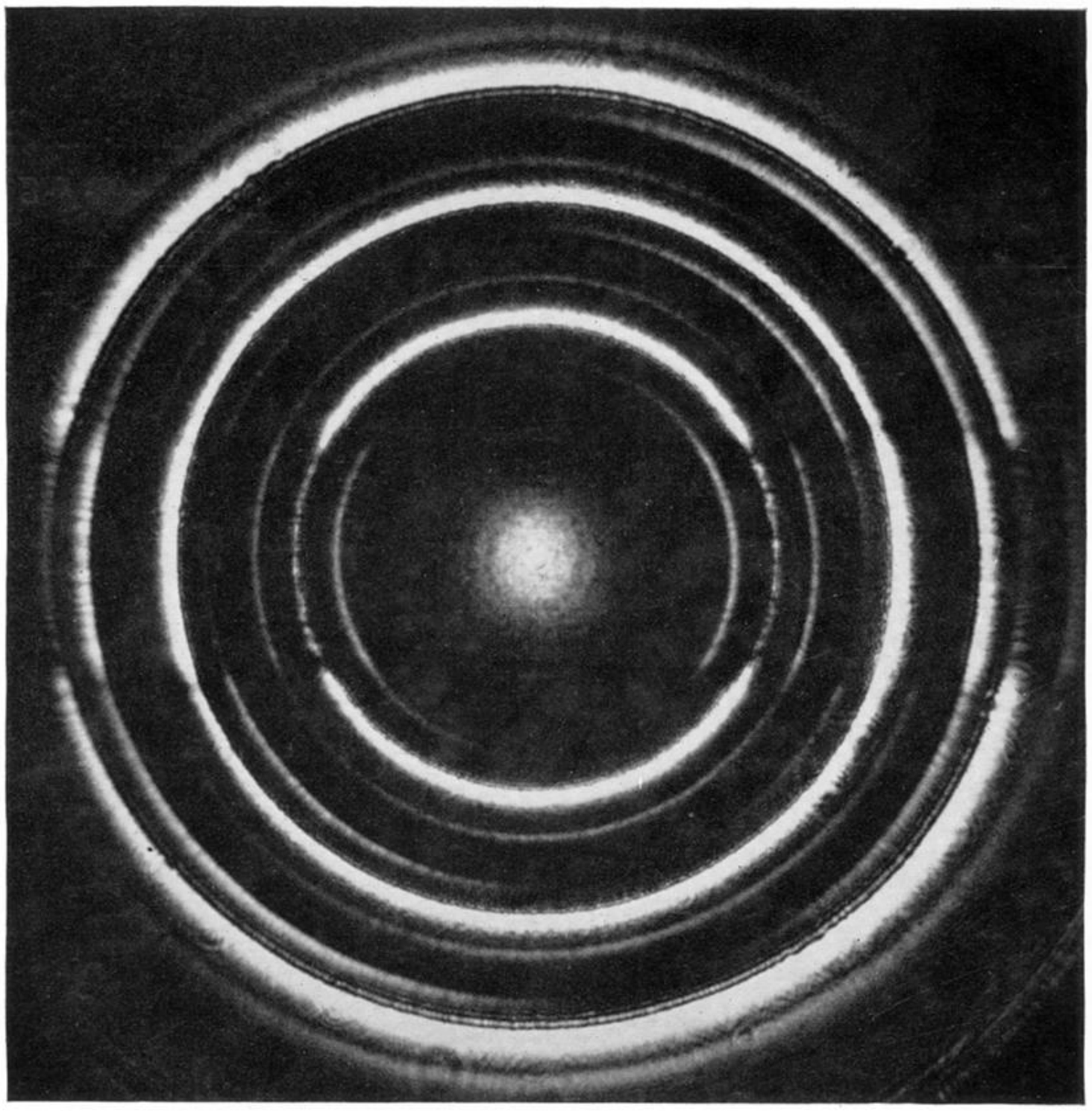

(*a*)

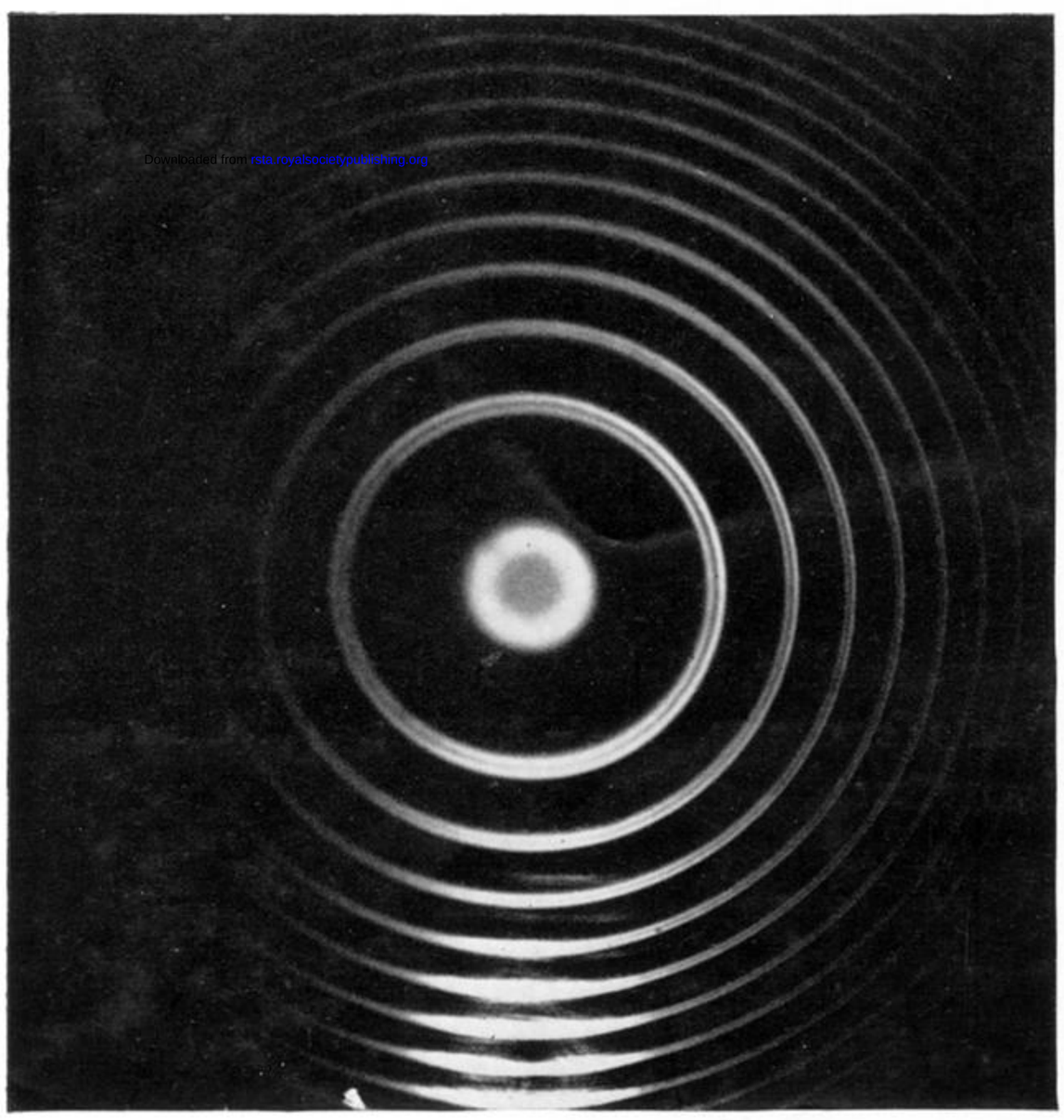

(*b*)

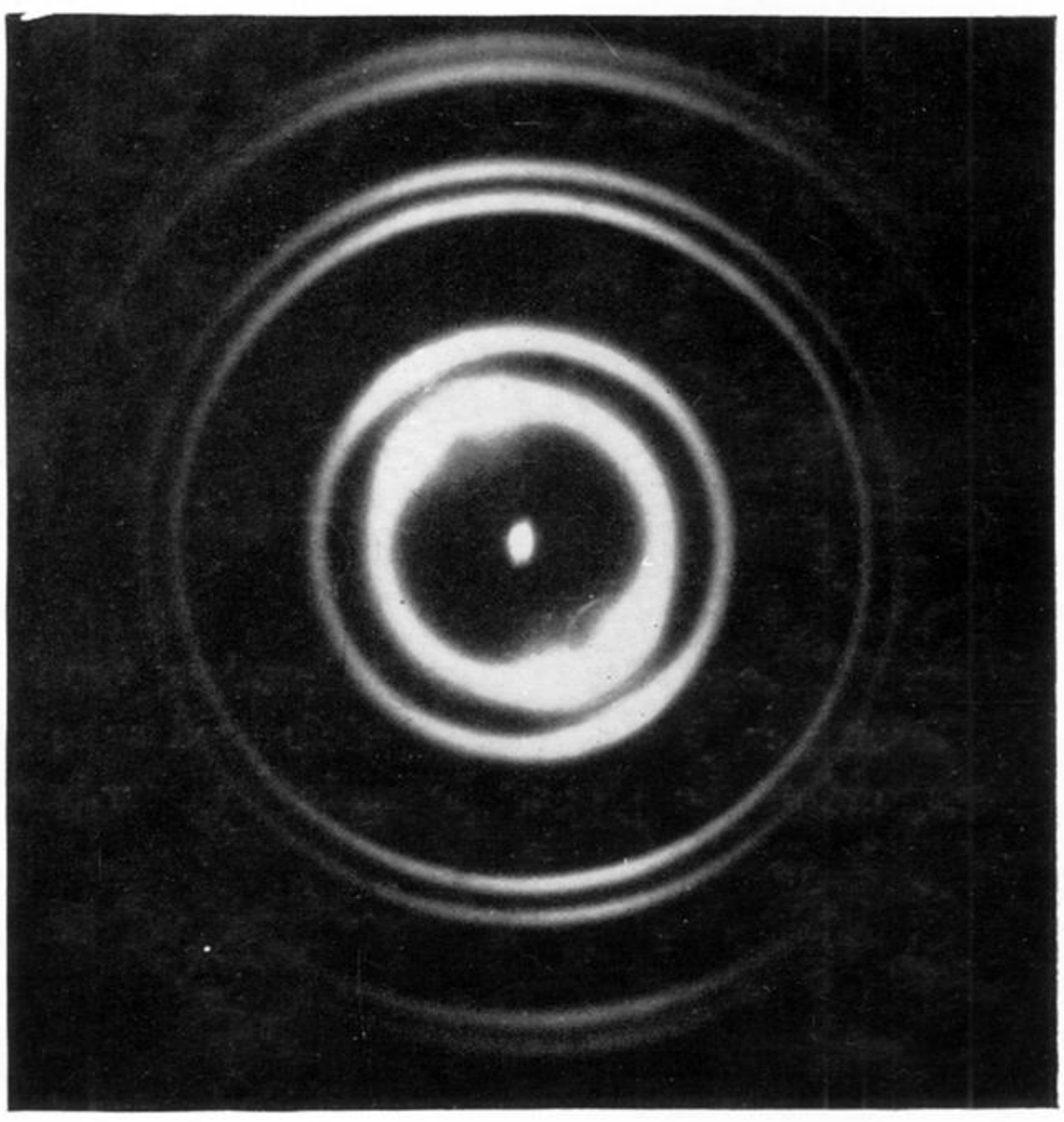

(*c*)

PHILOSOPHICAL TRANSACTIONS OF THE ROYAL SOCIETY A MATHEMATICAL, PHYSICAL & ENGINEERING SCIENCES

FIGURE 13. (*a*) Effect of blocking off a segment of the interferometer input aperture. Interferogram of gas laser operating on three longitudinal modes showing alternation in fringe intensities along diametral section due to spatial coherence of the laser modes.
(*b*), (*c*) Simultaneous interferograms of two longitudinal modes of a gas laser taken with 10 cm gap (*b*) plane and (*c*) defocused spherical mirror etalons respectively.